Ultra-high-pressure generation in the relativistic transparency regime in laser-irradiated nanowire arrays

J. F. Ong, P. Ghenuche, I. C. Edmond Turcu, A. Pukhov, and K. A. Tanaka

Ultra-high-pressure generation in the relativistic transparency regime in laser-irradiated nanowire arrays

J. F. Ong [1,*], P. Ghenuche [1], I. C. Edmond Turcu,[1,2] A. Pukhov,[3] and K. A. Tanaka [1,4,†]

[1]*Extreme Light Infrastructure - Nuclear Physics (ELI-NP), "Horia Hulubei" National Institute for Physics and Nuclear Engineering (IFIN-HH), 30 Reactorului Street, RO-077125 Bucharest-Măgurele, Romania*
[2]*UKRI/STFC Central Laser Facility, Rutherford Appleton Laboratory, Harwell Campus, Didcot, Oxfordshire OX11 0QX, United Kingdom*
[3]*Institut für Theoretische Physik, Heinrich-Heine-Universität Düsseldorf, D-40225 Düsseldorf, Germany*
[4]*Institute of Laser Engineering, Osaka University, Yamada-oka 2-6, Suita, Osaka 565-0871, Japan*

We show that an ultra-high-pressure plasma can be generated when an aligned nanowire is irradiated by a laser with relativistic transparent intensity. Using a particle-in-cell simulation, we demonstrate that the expanded plasma following the z pinch becomes relativistically transparent and compressed longitudinally by the oscillating component of the ponderomotive force. The compressed structure persists throughout the pulse duration with a maximum pressure of 40 Tbar when irradiated with a laser at an intensity of 10^{23} W cm^{-2}, $5\times$ higher than the z-pinch pressure. These results suggest an alternative approach to extending the current attainable pressure in the laboratory.

I. INTRODUCTION

Matter under ultra-high pressure is crucial in the advancement of inertial confinement fusion [1–3] and the study of warm dense matter [4,5]. This type of matter can be found in the interiors of planets and stars with Mbar-to-Gbar pressures [6,7]. Gigabar pressures can be achieved in the laboratory using a laser-based method [8–11]. Terabar pressures were predicted when a nanowire target is irradiated with an ultraintense laser. [12,13]. The formation of a high-pressure environment using z pinch and the associated instability has been extensively discussed in magnetic confinement fusion [14,15] or pulsed-power accelerators [16,17].

Aligned nanowires heated with a 0.6 J laser pulse were demonstrated to achieve a pressure of 125 Gbar [12]. The strong laser irradiation of a nanowire array provides a unique z pinch capable of compressing a solid to $100\times$ its initial mass density [18]. The scaling of solid compression against laser intensity using a particle-in-cell (PIC) simulation shows that the radius of the nanowire can be compressed down to $0.1\times$ its initial radius with $a_0 = 17$. Here, $a_0 = eE_0/(mc\omega_L)$ is the normalized laser amplitude, where E_0 is the peak laser field strength, ω_L is the laser angular frequency, and e and m are the charge and mass of the electron. PIC simulations also show that energy densities in excess of 80 GJ cm^{-3} could be obtained in the expanding plasma with a laser intensity of 10^{22} W cm^{-2} ($a_0 = 34$), reaching pressures of 350 Gbar [12]. Further, scaling to 7 Tbar pressure was predicted. A similar simulation indicates that the energy density of 0.1 TJ cm^{-3} can be obtained by irradiating a laser with an intensity of 10^{23} W cm^{-2} onto a foam target made of disordered carbon nanowires [13]. The pressure obtained with a nanowire array is comparable to the laser ICF and Z-machine at Sandia National Laboratory [19–21], which is of order Gbar but with a more compact setup.

Typically, the nanowire z pinch occurs during the rising edge of an ultraintense femtosecond laser pulse and produces an ultradense electron bunch of 1–2 μm length that propagates with the laser along the nanowires. Then, the compressed nanowire expands to fill the void rapidly, limiting further laser penetration. However, the onset of relativistic self-induced transparency (RT) when the peak of the laser pulse arrives with higher intensities allows further laser penetration. Experiments with a plane or nanowire target in the RT regime have been demonstrated to improve the ion acceleration [22–24]. To our knowledge, the plasma pressure of laser-irradiated solid targets under the RT regime has yet to be identified. The use of nanowires may lead to different phenomena that warrant further investigation.

In this paper, we present ultra-high-pressure generation when an aligned nanowire is irradiated with a laser pulse of relativistic transparent intensity. We show that the transparent plasma following the z pinch is compressed by the oscillating component of the ponderomotive force. This results in the formation of periodic plasma layers separated by $\lambda_L/2$. Our simulation shows that the pressure of these plasma layers reaches 40 Tbar, $5\times$ higher than the pressure generated by a z pinch when irradiated with a laser of intensity 10^{23} W cm^{-2}. Since the z pinch is absent in the RT regime, the limitation characterizing the pressure such as a kink instability is no longer relevant. Ultra-high-pressure plasma layers persist for the whole duration of the laser pulse and remain in Tbar pressures within 100 fs. This regime suggests an alternative approach for generating ultra-high pressure to the subpetabar regime.

*jianfuh.ong@eli-np.ro
†kazuo.tanaka@eli-np.ro
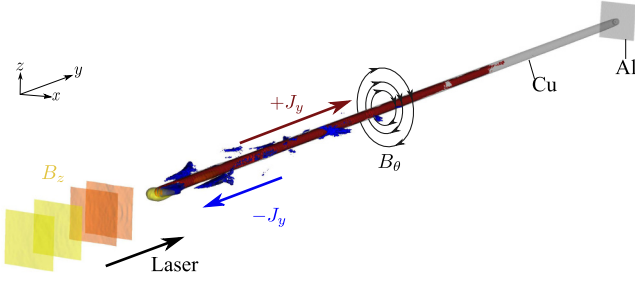
FIG. 1. 3D PIC simulation of ultra-high-pressure formation by an intense laser pulse with a copper nanowire attached to the aluminum substrate. Electrons are ionized from the surface and move in the forward direction (blue, forward current). The colored arrows indicate the direction of the current while electrons move in the reverse direction. A return current is created (red). The quasistatic azimuthal magnetic field B_θ pinches the nanowire.

II. METHODS

We performed full three-dimensional relativistic particle-in-cell (PIC) simulations using the PICONGPU code [25] version 5.0.0. The code consists of a standard PIC algorithm in which the ponderomotive effects are included naturally. The code is extended by taking into account the strong field ionization [26,27], and radiation reaction [28].

The simulation box has dimensions of $x \times y \times z = 0.5 \times 7.0 \times 0.5\ \mu m^3$ with spatial resolution $\Delta x \times \Delta y \times \Delta z = 7.8 \times 1.97 \times 7.8\ nm^3$, and time step $\Delta t = 3.78$ as. The number of particles per cell for the ion species is four while the fourth-order particle shape function and current smoothing were used to suppress the numerical heating. The initial charge state of the ion is zero, and a mobile ion is implemented. The strong field ionization was treated by tunneling and barrier-suppression ionization [26,27]. The simulations were performed with 16 Nvidia® V100 GPUs.

The nanowire was modeled as a copper rod with length $L = 5\ \mu m$ and diameter $d = 100$ nm, attached to a 0.5-μm-thick aluminum substrate as shown in Fig. 1. The copper nanowire has a steplike profile with a mass density $\rho_0 = 8.96\ g\,cm^{-3}$ ($n_i = 50 n_{cr}$). The neighboring nanowire was represented using periodic lateral boundary conditions. The described z-pinch mechanism is also illustrated.

Since the present simulations consider the interaction within a small area, the laser pulse was modeled as a linearly polarized plane wave with a central wavelength $\lambda_L = 0.8\ \mu m$. The laser peak intensity is $I_0 = 10^{23}\ W\,cm^{-2}$ ($a_0 = 215$) and irradiated onto the nanowire at normal incidence. Here, $a_0 = eE_0/(mc\omega_L)$ is the normalized laser amplitude, where E_0 is the peak laser field strength, $\omega_L = 2\pi/\lambda_L$ is the laser central frequency, and e and m being the charge and mass of the electron. The laser intensity temporal profile is Gaussian, i.e., $E_0(y) = E_0 \exp[-(y - ct)^2/4\tau_L^2]$, where $\tau_L = \tau_{FWHM}/(2\sqrt{2\ln 2})$, with pulse duration at full width at half maximum (FWHM), $\tau_{FWHM} = 22$ fs. The peak of the laser pulse is at the tip of the nanowire at $t = 0$ and propagates in the $+y$ direction. The peak laser intensity is chosen to be large enough for the onset of RT to overdense plasma.

The pressure for equilibrium relativistic gas is derived from relativistic hydrodynamics, and Ryu *et al.* [29] provides a simple approximation as

$$\frac{p}{\varepsilon} = \frac{1 - \delta + \sqrt{1 + 6\delta + \delta^2}}{6}, \qquad (1)$$

where ε is the kinetic energy density, and $\delta = \rho c^2/\varepsilon$ is the ratio of rest mass energy density to kinetic energy density. Here, ρ is the rest mass density. For ultrarelativistic gas, $\varepsilon \to \infty$, and $p = \varepsilon/3$, while for nonrelativistic gas, $\varepsilon \to 0$, and $p = 2\varepsilon/3$.

The radiation emission via a strong field interaction was included. The radiation emission is modeled with synchrotron radiation, which incorporates the quantum electrodynamics (QED) correction. Electron energy losses and radiation reaction were self-consistently calculated. Only photons with an oscillation period less than a grid size were calculated. For brevity, details of the radiation emission in a strong field can be referred to Ref. [30]. A discussion of gamma-ray emission is out of the scope of this paper and will be presented elsewhere.

III. RESULTS AND DISCUSSION

A. Energy density and pressure

First, we examine the evolution of energy density. With such a high laser intensity, the surface electrons of the nanowire are rapidly ionized by the rising edge of the laser pulse as shown in Fig. 2. At $t = -24$ fs, the laser intensity at the nanowire tip is already $1.2 \times 10^{20}\ W\,cm^{-2}$. The peak intensity will reach the tip at $t = 0$. The ionized electrons are ripped off and accelerated toward the substrate. Part of the electrons enter the nanowire and excite a plasma wakefield [31]. The z pinch has already begun at $t = -17$ fs, and the energy density reaches the order of 1 TJ cm^{-3}. The ultradense electron bunch is propagating toward the substrate, and the nanowire tip expands. At the tip, the peak energy density is 3.75 TJ cm^{-3}.

As the peak intensity approaches the nanowire tip, the plasma becomes transparent to the laser field due to relativistic self-induced transparency. The plasma is transparent when $n_e < \gamma n_{cr}$, where $\gamma = (1 + a_0^2/2)^{1/2}$, and $n_{cr} = \epsilon_0 m\omega_L^2/e^2$ is the critical density. Here, the relativistic critical density is $\gamma n_{cr} = 2.65 \times 10^{23}\ cm^{-3}$. After the z-pinch stage, the laser pulse continues to penetrate deep into the target even if the plasma has filled the void between the nanowires. Then, periodic ultra-high-energy-density plasma layers are formed inside the laser field as shown in Fig. 2 at $t = 2$ fs with a maximum energy density 115 TJ cm^{-3}. The maximum pressure is estimated to be 40 Tbar. The electron density of the ultradense bunch has now exceeded $10\,000 n_{cr}$, but its energy density is lower than that of the plasma layers and remain opaque to the laser. The plasma layers have a separation of $\sim\lambda_L/2$ and are formed via laser density modulation by the ponderomotive force (Fig. 2 at $t = 18$ fs). The layers persist for the whole duration of the laser pulse and cover the whole length of the nanowire. The plasma across the nanowire starts to become homogeneous from $t = 100$ fs with an energy density of the order of $\sim$800 GJ cm^{-3}. We then estimate the plasma
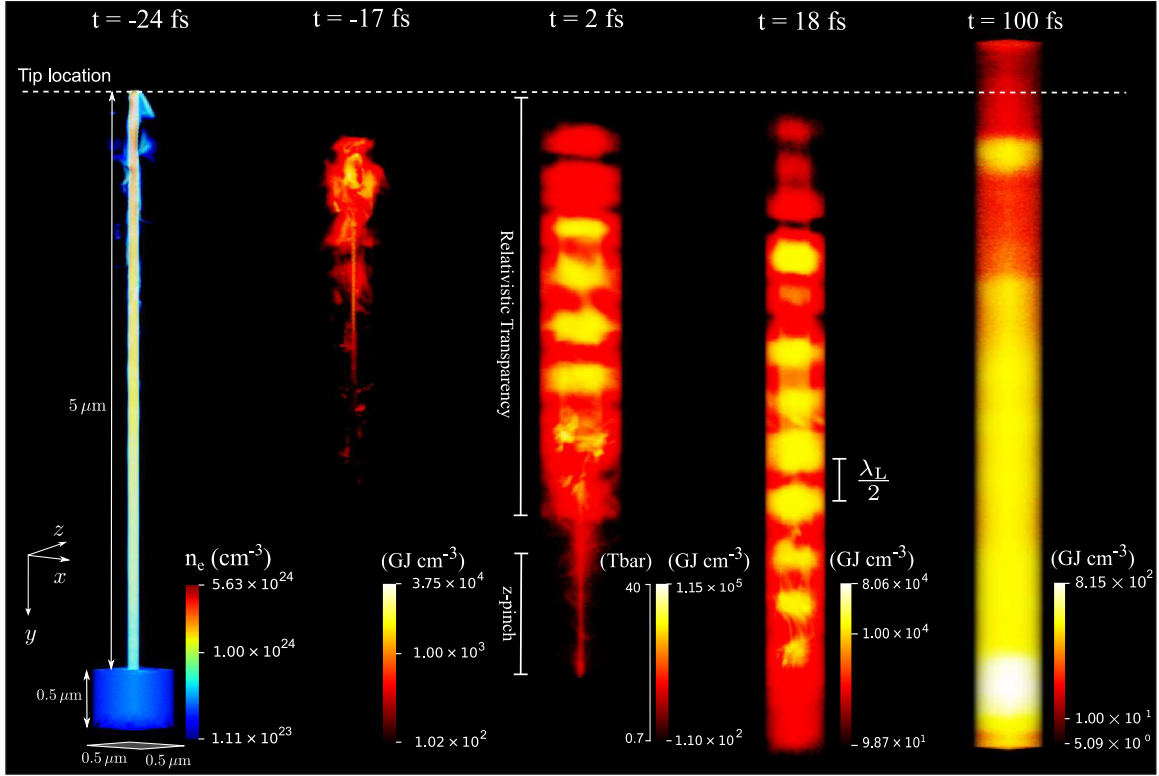
FIG. 2. The 3D density and kinetic energy density distribution of 100-nm-diameter Cu nanowire irradiated by a laser with intensity 10^{23} W cm^{-2} at $t = -24, -17, 2, 18,$ and 100 fs. The peak of the laser pulse reaches the tip of the nanowire at $t = 0$, indicated by the dashed line. The laser pulse is propagating in the $+y$ direction. The RT regime led to the plasma modulation with a period of $\lambda_L/2$ which is stable throughout the duration of the laser pulse. The pressure scale at $t = 2$ fs is an estimation based on Ryu *et al.* [29] in ultrarelativistic and nonrelativistic limits.

pressure from the kinetic energy density with a simple approximation given by Ryu *et al.* [29], which is accurate to 1%. We computed the pressure map together with the components
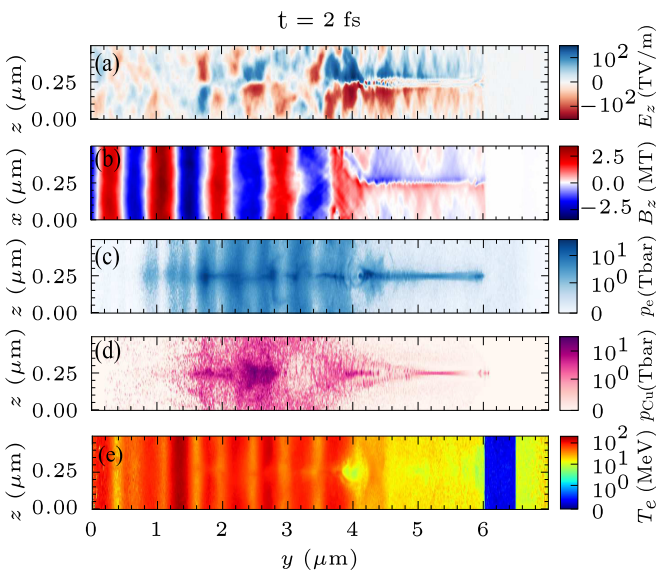
FIG. 3. The longitudinal cross section of (a) electric field component E_z, (b) magnetic field component B_z, (c) electron pressure, (d) ion pressure, and (e) electron temperature at $t = 2$ fs for laser intensity 10^{23} W cm^{-2}.

of the electromagnetic fields and temperature for a detailed distribution. Figure 3(a) shows the transverse electric field E_z at $t = 2$ fs. The charge separation field can be seen between $y = 1$ and 4 µm, while the electric field between $y = 4$ and 6 µm is radially outward, similar to the current carrying wire. Figure 3(b) shows the magnetic component B_z, where the alternating component of the laser is between $y = 1$ and 4 µm and the quasistatic field on the right surrounding the nanowire. This quasistatic magnetic field reaches 0.7 MT (7 gigagauss). Figure 3(c) shows the electron pressure map with the z pinch located between $y = 4$ and 6 µm. The periodic structure of pressure can be seen between $y = 1$ and 4 µm, where the peaks are located at a minimum of B_z. Here, the plasma is fully transparent to the laser fields. The ions also exhibit pinching as shown in Fig. 3(d), but the expansion is slower and located mainly around the center. The charge separation field pulls the electron back transversely, resulting in a higher electron pressure at the center than at the boundary. The electron temperature of the plasma layers reaches 100 MeV while the temperature of the z-pinch regime is one order smaller as shown in Fig. 3(e).

B. z-pinch regime

In the z-pinch regime, the pressure profile can be described by Bennett's equilibrium, $p(r) \propto I_0^2 R_0^2/(r^2 + R_0^2)^2$, where I_0 is the return current and $R_0 = 2\sqrt{2}\lambda_D(c/v_y)(1 + T_i/ZT_e)^{1/2}$ is the characteristic radius [32,33] [see Supplemental Material
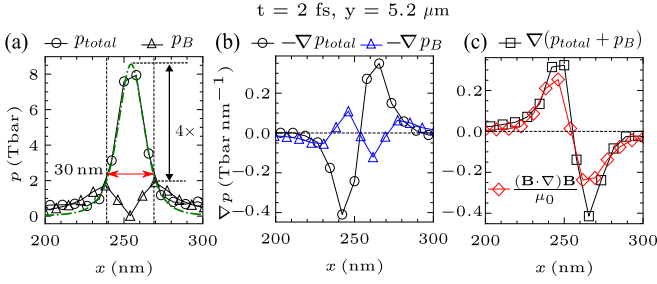
FIG. 4. (a) The lineout of the total plasma pressure p_{total} and magnetic pressure p_B at $t = 2$ fs and $y = 5.19$ μm. The green line is the pressure profile according to Bennett's equilibrium. The vertical dashed lines indicate the boundaries where $p_{total} = p_B$. The maximum p_{total} is $4\times$ the maximum of p_B. (b) The corresponding pressure forces where the negative values indicate the direction of the forces. (c) The total pressure force and magnetic tension force.

(SM) for the derivation [34]]. The pinch radius shrinks to the order of Debye's lengths $\lambda_D = (\epsilon_0 k_B T_e / n_e e^2)^{1/2}$ when the return current in which the fast electron is relativistic. That is to say, the peak pressure of a z pinch is limited by the Debye's length and the return current. Here, the maximum attainable pressure is ~ 8 Tbar. Figure 4(a) shows the total plasma pressure and the magnetic pressure across the ultradense bunch at $t = 2$ fs ($y = 5.2$ μm). The profile agrees with the simulation with $R_0 = 15$ nm and $I_0 = 0.11$ MA as depicted by the green line. The magnetic pressure increases linearly from the center to $r = R_0 \sim 15$ nm, where the plasma and magnetic pressures are in equilibrium and then fall off by $1/r$. The total plasma pressure at the center is approximately $4\times$ the magnetic pressure at $r = R_0$. Figure 4(b) shows the plasma pressure force $-\nabla p$ and the magnetic pressure force $-\nabla p_B$. Each pressure at $r \gtrsim R_0$ produces a radially outward force. Nevertheless, the magnetic pressure is less than the plasma pressure and insufficient to confine the ultradense bunch. The confinement force is attributed to the mechanical tension of the magnetic field line. The pressure balance for the ultradense bunch is evident in Fig. 4(c), where the total plasma and magnetic pressure forces are approximately equal to the magnetic tension force.

C. Relativistic transparency regime

In the RT regime, the electron plasma is confined longitudinally to form layers separated by half wavelength. Figure 5(a) shows the total plasma pressure along the center of the simulation box, with the ponderomotive pressure. The maxima of the plasma pressure are located at the minima of the ponderomotive pressure. Here, the maximum plasma pressure is 40 Tbar, $5\times$ higher than the z pinch. The longitudinal confinement or the ponderomotive pressure is attributed to the $J \times B$ heating [35] which operates in the RT regime, where J is the electron current due to the laser electric field, $E(y, t) = E_0(y)\hat{x}\sin(\omega_L t)$, $E_0(y)$ is the longitudinal laser profile, and B is the laser magnetic field. This longitudinal force is $f_y \propto -\partial E_0^2(y)/\partial y \times (1 - \cos 2\omega_L t)\hat{y}$, where the cycle average is the ponderomotive force. The second term explains the formation of the plasma layers separated by a $\lambda_L/2$ interval or $2\omega_L$ frequency. The compression force is acting from both sides of each layer as evident in Fig. 5(b). For an opaque plasma,
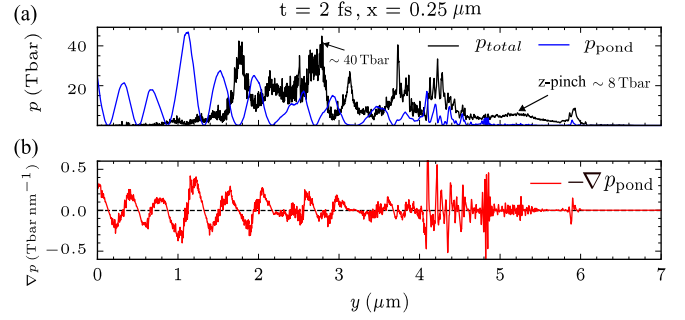
FIG. 5. (a) The lineout of the total plasma pressure p_{total} and ponderomotive pressure p_{pond} at $t = 2$ fs and $x = 0.25$ μm. The maximum pressure due to RT is up to ~ 40 Tbar, $5\times$ of the z pinch. (b) The oscillating ponderomotive forces, which show the compression toward each plasma layer.

the $2\omega_L$ fast electron bunches are generated at the tip of the nanowire without exhibiting periodic density layers [31]. The ponderomotive pressure can be readily obtained as $p_{pond} = \epsilon_0 n_e/(4n_{cr}) \times E_0^2(1 - \cos 2\omega_L t)$, such that the force per unit volume is $F_y = n_e f_y = -\nabla p_{pond}$. If the ratio n_e/n_{cr} is set to $\lesssim a_0/\sqrt{2}$ for a relativistically transparent plasma, one can then obtain the upper limit of pressure as $p_{pond} < (mc^2/2\sqrt{2})a_0^3 n_{cr}$ or in an engineering formula as $p_{pond} < 0.32 a_0^3/\lambda_{L,\mu m}^2$ Gbar, where $\lambda_{L,\mu m}$ is the laser wavelength in micrometers. The maximum possible pressure is depending only on the laser parameters. For $a_0 = 215$, the maximum possible pressure in RT can be up to $p < 5$ Pbar. To increase the maximum plasma pressure in the RT regime, the nanowire can be irradiated with a higher laser intensity or frequency-doubled/tripled laser. However, it remains unclear whether the radiation loss via the effects of radiation reaction would be the limiting factor. In addition, enlarging both the length and diameter of the nanowire would expand the high-pressure volume, but they are limited by the laser spot size and Rayleigh length. These details are of interest and can be studied further in the future.

We note that the plasma layers are absent for a circularly polarized laser pulse, where the term consisting of $2\omega_L$ vanishes. The plasma layers are not formed as shown in Fig. 6. The maximum attainable plasma pressure is also lower for a CP laser with a pressure cavity formed at the center along the nanowire.
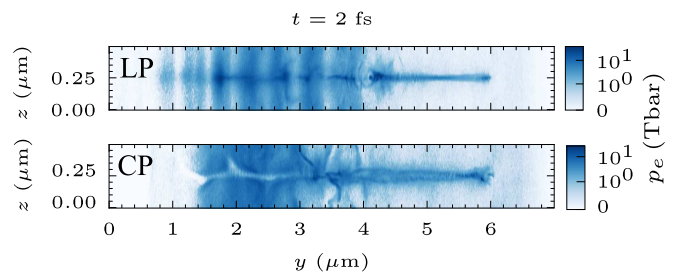
FIG. 6. The comparison of electron pressure generated by using linearly polarized (LP) and circularly polarized (CP) laser pulses.
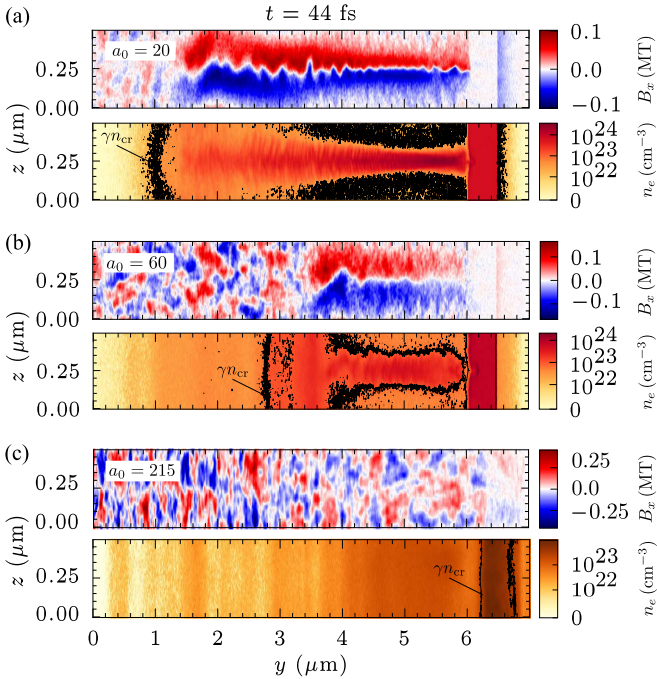
FIG. 7. The transition between the z-pinch instability regime and the stable RT regime. Longitudinal cross section in the y-z plane for magnetic field component B_x and electron density n_e for (a) $a_0 = 20$, (b) $a_0 = 60$, and (c) $a_0 = 215$ at t = 44 fs. The black lines are the boundaries of the relativistic critical density γn_{cr}.

D. Instabilities

At lower laser intensities, the plasma instabilities dominate as shown in Fig. 7(a). A series of simulations with different laser intensities were performed. For $a_0 = 20$, the pinching begins at a slower rate, and the instability develops after the laser pulse ends. The magnetic field imbalance displaces the nanowire and forms the kink instability, which is clearly shown in Fig. 7(a) by the kink in B_x and electron density. However, the laser field could not penetrate the plasma and the instabilities are preserved (see also SM Fig. S1 [34]). For $a_0 = 60$ [Fig. 7(b)], the pinching begins at a faster rate, and the instability does not form due to the stronger laser field. The strong ponderomotive force pushes the relativistic critical density surface ($n_e \sim 42 n_{cr}$) forward and the transparent plasma is left behind forming high-pressure layers. Part of the laser field is reflected off the critical surface and undergoes a redshift. For higher laser intensities, this process occurred at a faster rate where the z pinch ended and formed multiple plasma layers, as depicted in Fig. 7(c). In this regime, we see stable modulating layers lasting >20 fs and resulting in pressure >10 Tbar (see also SM Figs. S2 and S3 [34]). It is of interest to gain insight into how the pressure changes with the laser intensity. We compare the temporal evolution of the total average pressure for different laser intensities in Fig. 8 up to 100 fs of interaction time. The pressure rise time becomes shorter with increasing laser intensities. The z pinch typically begins at $t < 0$. The pressure increment is slower for $a_0 = 20$ and reaches 0.1 Tbar at $t = 20$ fs. After that, the kink instability dominates and the pressure gradually reduces.
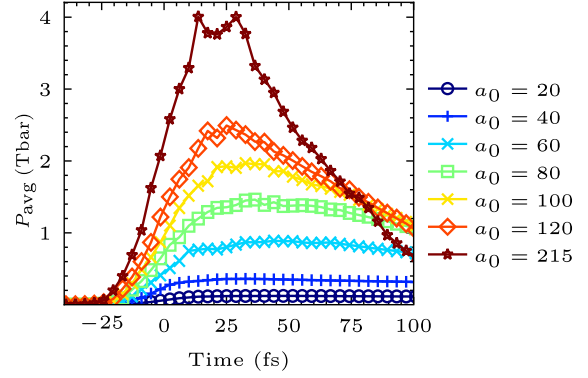
FIG. 8. The evolution of total average pressure for different laser intensities.

For $a_0 = 40$, 60, and 80 the pressure increases to 0.4, 0.9, and 1.4 Tbar, respectively, and remains constant for about 20 fs. At this point, the plasma layers start to form, and their pressure exceeds the z pinch. An even higher average pressure can be obtained when the laser intensity is further increased to $a_0 = 100$ and 120, approaching 2.4 Tbar. The total average pressure at $a_0 = 215$ reaches 4 Tbar. The FWHM duration of the ultra-high pressure is roughly 100 fs.

IV. CONCLUSIONS

In conclusion, 40 Tbar pressures are predicted when an aligned nanowires are irradiated with a laser in the RT regime. The periodic pressure structure stretches the full 5 μm length of the nanowire and lasts for the full duration of the laser pulse. The RT regime removes the limit on the maximum attainable pressure, as well as the limiting spatial instabilities associated with the nanoscale z pinch. This regime could extend the maximum pressures attainable in the laboratory beyond Tbar. The regime opens the possibility to obtain ultra-high pressure that could not be achieved by using z pinch for the studies in microscale nuclear fusion, and warm dense matter, as well as extending the equation of state research to the subpetabar regime. The simulation results also provide insight into the pressure sustainability at different laser intensities for optimization in microscale nuclear fusion experiments. To our knowledge, these results provide clear evidence of the existence of regimes different from the existing z pinch when the nanowire array is irradiated at sufficiently high laser intensities. Although the pinching mechanism is similar to the ones in the Sandia-type large z-pinch machine [36], the nanowire is special for the deep penetration depth, which allows the switching between different regimes by increasing the laser intensities to the RT regime.

[1] R. Betti and O. A. Hurricane, Inertial-confinement fusion with lasers, Nat. Phys. **12**, 435 (2016).

[2] T. Gong, H. Habara, K. Sumioka, M. Yoshimoto, Y. Hayashi, S. Kawazu, T. Otsuki, T. Matsumoto, T. Minami, K. Abe, K. Aizawa, Y. Enmei, Y. Fujita, A. Ikegami, H. Makiyama, K. Okazaki, K. Okida, T. Tsukamoto, Y. Arikawa, S. Fujioka *et al.*, Direct observation of imploded core heating via fast electrons with super-penetration scheme, Nat. Commun. **10**, 5614 (2019).

[3] F. Zhang, H. B. Cai, W. M. Zhou, Z. S. Dai, L. Q. Shan, H. Xu, J. B. Chen, F. J. Ge, Q. Tang, W. S. Zhang, L. Wei, D. X. Liu, J. F. Gu, H. B. Du, B. Bi, S. Z. Wu, J. Li, F. Lu, H. Zhang, B. Zhang *et al.*, Enhanced energy coupling for indirect-drive fast-ignition fusion targets, Nat. Phys. **16**, 810 (2020).

[4] M. Koenig, A. Benuzzi-Mounaix, A. Ravasio, T. Vinci, N. Ozaki, S. Lepape, D. Batani, G. Huser, T. Hall, D. Hicks, A. MacKinnon, P. Patel, H. S. Park, T. Boehly, M. Borghesi, S. Kar, and L. Romagnani, Progress in the study of warm dense matter, Plasma Phys. Controlled Fusion **47**, B441 (2005).

[5] D. Riley, Generation and characterisation of warm dense matter with intense lasers, Plasma Phys. Controlled Fusion **60**, 014033 (2018).

[6] T. Guillot, Interiors of giant planets inside and outside the solar system, Science **286**, 72 (1999).

[7] N. Nettelmann, B. Holst, A. Kietzmann, M. French, R. Redmer, and D. Blaschke, *Ab initio* equation of state data for hydrogen, helium, and water and the internal structure of Jupiter, Astrophys. J. **683**, 1217 (2008).

[8] R. Cauble, D. W. Phillion, T. J. Hoover, N. C. Holmes, J. D. Kilkenny, and R. W. Lee, Demonstration of 0.75 Gbar planar shocks in x-ray driven colliding foils, Phys. Rev. Lett. **70**, 2102 (1993).

[9] K. U. Akli, S. B. Hansen, A. J. Kemp, R. R. Freeman, F. N. Beg, D. C. Clark, S. D. Chen, D. Hey, S. P. Hatchett, K. Highbarger, E. Giraldez, J. S. Green, G. Gregori, K. L. Lancaster, T. Ma, A. J. MacKinnon, P. Norreys, J. Pasley, N. Patel, C. Shearer *et al.*, Laser Heating of Solid Matter by Light-Pressure-Driven Shocks at Ultrarelativistic Intensities, Phys. Rev. Lett. **100**, 165002 (2008).

[10] R. Nora, W. Theobald, R. Betti, F. J. Marshall, D. T. Michel, W. Seka, B. Yaakobi, M. Lafon, C. Stoeckl, J. Delettrez, A. A. Solodov, A. Casner, C. Reverdin, X. Ribeyre, A. Vallet, J. Peebles, F. N. Beg, and M. S. Wei, Gigabar Spherical Shock Generation on the OMEGA Laser, Phys. Rev. Lett. **114**, 045001 (2015).

[11] S. Y. Gus'kov, P. A. Kuchugov, and G. A. Vergunova, Extreme matter compression caused by radiation cooling effect in gigabar shock wave driven by laser-accelerated fast electrons, Matter Radiat. Extremes **6**, 020301 (2021).

[12] C. Bargsten, R. Hollinger, M. G. Capeluto, V. Kaymak, A. Pukhov, S. Wang, A. Rockwood, Y. Wang, D. Keiss, R. Tommasini, R. London, J. Park, M. Busquet, M. Klapisch, V. N. Shlyaptsev, and J. J. Rocca, Energy penetration into arrays of aligned nanowires irradiated with relativistic intensities: Scaling to terabar pressures, Sci. Adv. **3**, e1601558 (2017).

[13] K. Jiang, A. Pukhov, and C. T. Zhou, TJ cm^{-3} high energy density plasma formation from intense laser-irradiated foam targets composed of disordered carbon nanowires, Plasma Phys. Controlled Fusion **63**, 015014 (2021).

[14] U. Shumlak, R. P. Golingo, B. A. Nelson, and D. J. Den Hartog, Evidence of Stabilization in the Z-Pinch, Phys. Rev. Lett. **87**, 205005 (2001).

[15] U. Shumlak and C. W. Hartman, Sheared Flow Stabilization of the $m = 1$ Kink Mode in Z Pinches, Phys. Rev. Lett. **75**, 3285 (1995).

[16] M. K. Matzen, Z pinches as intense x-ray sources for high-energy density physics applications, Phys. Plasmas **4**, 1519 (1997).

[17] M. G. Haines, P. D. LePell, C. A. Coverdale, B. Jones, C. Deeney, and J. P. Apruzese, Ion Viscous Heating in a Magnetohydrodynamically Unstable Z Pinch at over 2×10^9 Kelvin, Phys. Rev. Lett. **96**, 075003 (2006).

[18] V. Kaymak, A. Pukhov, V. N. Shlyaptsev, and J. J. Rocca, Nanoscale Ultradense Z-Pinch Formation from Laser-Irradiated Nanowire Arrays, Phys. Rev. Lett. **117**, 035004 (2016).

[19] S. E. Wurzel and S. C. Hsu, Progress toward fusion energy breakeven and gain as measured against the Lawson criterion, Phys. Plasmas **29**, 062103 (2022).

[20] S. Le Pape, L. F. Berzak Hopkins, L. Divol, A. Pak, E. L. Dewald, S. Bhandarkar, L. R. Bennedetti, T. Bunn, J. Biener, J. Crippen, D. Casey, D. Edgell, D. N. Fittinghoff, M. Gatu-Johnson, C. Goyon, S. Haan, R. Hatarik, M. Havre, D. D-M. Ho, N. Izumi *et al.*, Fusion Energy Output Greater than the Kinetic Energy of an Imploding Shell at the National Ignition Facility, Phys. Rev. Lett. **120**, 245003 (2018).

[21] M. R. Gomez, S. A. Slutz, P. F. Knapp, K. D. Hahn, M. R. Weis, E. C. Harding, M. Geissel, J. R. Fein, M. E. Glinsky, S. B. Hansen, A. J. Harvey-Thompson, C. A. Jennings, I. C. Smith, D. Woodbury, D. J. Ampleford, T. J. Awe, G. A. Chandler, M. H. Hess, D. C. Lamppa, C. E. Myers *et al.*, Assessing stagnation conditions and identifying trends in magnetized liner inertial fusion, IEEE Trans. Plasma Sci. **47**, 2081 (2019).

[22] B. M. Hegelich, I. Pomerantz, L. Yin, H. C. Wu, D. Jung, B. J. Albright, D. C. Gautier, S. Letzring, S. Palaniyappan, R. Shah, K. Allinger, R. Hörlein, J. Schreiber, D. Habs, J. Blakeney, G. Dyer, L. Fuller, E. Gaul, E. Mccary, A. R. Meadows *et al.*, Laser-driven ion acceleration from relativistically transparent nanotargets, New J. Phys. **15**, 085015 (2013).

[23] A. A. Sahai, F. S. Tsung, A. R. Tableman, W. B. Mori, and T. C. Katsouleas, Relativistically induced transparency acceleration of light ions by an ultrashort laser pulse interacting with a heavy-ion-plasma density gradient, Phys. Rev. E **88**, 043105 (2013).

[24] A. Curtis, R. Hollinger, C. Calvi, S. Wang, S. Huanyu, Y. Wang, A. Pukhov, V. Kaymak, C. Baumann, J. Tinsley,

V. N. Shlyaptsev, and J. J. Rocca, Ion acceleration and D-D fusion neutron generation in relativistically transparent deuterated nanowire arrays, Phys. Rev. Res. **3**, 043181 (2021).

[25] H. Burau, R. Widera, W. Hönig, G. Juckeland, A. Debus, T. Kluge, U. Schramm, T. E. Cowan, R. Sauerbrey, and M. Bussmann, Picongpu: A fully relativistic particle-in-cell code for a GPU cluster, IEEE Trans. Plasma Sci. **38**, 2831 (2010).

[26] N. B. Delone and V. P. Krainov, Tunneling and barrier-suppression ionization of atoms and ions in a laser radiation field, Phys. Usp. **41**, 469 (1998).

[27] P. Mulser and D. Bauer, *High Power Laser-Matter Interaction*, Springer Tracts in Modern Physics (Springer, Berlin, 2010).

[28] H. Burau, Entwicklung und Überprüfung eines Photonenmodells für die Abstrahlung durch hochenergetische Elektronen, Ph.D. thesis, TU Dresden, 2016.

[29] D. Ryu, I. Chattopadhyay, and E. Choi, Equation of state in numerical relativistic hydrodynamics, Astrophys. J. Suppl. Ser. **166**, 410 (2006).

[30] T. G. Blackburn, Radiation reaction in electron–beam interactions with high-intensity lasers, Rev. Mod. Plasma Phys. **4**, 5 (2020).

[31] J. F. Ong, P. Ghenuche, and K. A. Tanaka, Electron transport in a nanowire irradiated by an intense laser pulse, Phys. Rev. Res. **3**, 033262 (2021).

[32] W. H. Bennett, Magnetically self-focussing streams, Phys. Rev. **45**, 890 (1934).

[33] M. G. Haines, A review of the dense Z-pinch, Plasma Phys. Controlled Fusion **53**, 093001 (2011).

[34] See Supplemental Material at http://link.aps.org/supplemental/10.1103/PhysRevE.107.065208 for derivation and extended data.

[35] W. L. Kruer and K. Estabrook, $J \times B$ heating by very intense laser light, Phys. Fluids **28**, 430 (1985).

[36] Z pulsed power facility, https://www.sandia.gov/z-machine/.